The study of Nuclear Mass Model by Sequential Least Squares Programming*

Hang Yang,[1] Chencun Yu,[1] Xuxiao Yu,[1] Amir Jalili,[1] Hankui Wang,[1,†] and Youbao Wang[2,‡]

[1]*School of Science, Zhejiang Sci-Tech University, Hangzhou 310018, China*
[2]*China Institute of Atomic Energy, P.O. Box 275(10), Beijing 102413, China*

Nuclear mass is an important property in both nuclear and astrophysics. Some algorithms are applied to improve the accuracy of the nuclear mass model. The algorithm of Sequential Least Squares Programming enhances the precision of multinomial mass models by reducing the error from 1.863 MeV to 1.631 MeV. We further test these algorithms by 200 samples of mass formulas selecting from the δE term of $E_{isospin}$ mass model. Among these algorithms, the Sequential Least Squares Programming has the best performance in both root mean square errors and computational efficiency. This algorithm is suitable to deal with large-scale, multi-parameter optimization tasks in nuclear physics.

Keywords: Nuclear mass model, binding energy, magic nuclei, sequential least squares algorithm

I. INTRODUCTION

An atomic nucleus contains valuable information about the atomic structure and is a fundamental physical property [1]. Changes in atomic mass directly affect nuclear stability and energy release during nuclear reactions [2]. The mass of a neutron-rich nucleus plays a crucial role in fast neutron capture (r-process) during stellar nucleosynthesis. Thus, studying the mass is essential for a comprehensive understanding of the formation and evolution of elements in the universe [3–5]. Recently, the development of radioactive ion beam facilities has led to experimental measurements of over 3000 ground state atomic masses [6, 7], with the study continuously expanding to both sides of the β-stability line. Astrophysics requires large amounts of data on the masses of neutron-rich or neutron-poor nuclei in regions far from the stability line. This is difficult to measure directly using current technology. Therefore, many different types of mass models have been proposed.

In 1935, Bethe-Weizsacker proposed the semiempirical BW2 mass formula [8–10] that predicts mass with an accuracy of approximately 3 MeV. In Ref. [11], nuclear binding energy divided into two parts: a large and smooth component along with a small and fluctuating component. The classical droplet model accounts only for the smooth trend and not the rapid fluctuation of the binding energy around the shell gap with a number of protons and neutrons. This suggests that important physical effects are absent in the classical mass model [12, 13]. To solve this problem, physicists have developed macroscopic-microscopic mass models. These models introduce shell correction terms, such as the finite force range droplet model (FRDM) [14], Koura-Tachibana-Uno-Yamada (KTUY) [15], Lublin Strasbourg drop (LSD) [16], and micromass models such as the Hartree-Fock-Bogoliubov (HFB) approach [17, 18] and relativistic mean-field theory (RMF) [19]. The cited research is primarily based on the density functional theory (DFT) [20]. Although DFT is more complex, it exhibits superior extrapolation capabilities.

Kirson et al. added six physical terms as multiple physical constraints to the mass model [21–27]. The BW2 mass model thus obtained was solved to some extent, addressing the problems of missing physics and overfitting that existed in early semi-empirical mass formulations, thereby reducing the root mean square error (RMSD) [28] to 1.92 MeV. Machine learning has important applications in nuclear physics because of its ability to handle complex problems, such as predicting half-life, charge radius, and charge density [29–32]. By considering the α-decay energy and Garvey-Kelson relations (GKs) and applying the multi-objective optimization (MOO) method [13, 33, 34], Qian and his research team significantly improved the theoretical accuracy of the BW2 model. Taking into account the isospin dependence, Bhagwat improved the liquid drop model to a model related to isospin and added fluctuation terms [35], which explained the binding energy of nucleons very well. Sequential least squares programming (SLSQP) [36] is a suitable algorithm for solving nonlinear optimization problems with constraints, as it can handle multiple constraints and nonlinear objective functions. SLSQP was initially applied to the layout of antenna arrays. Research has also demonstrated its feasibility and applicability to nuclear mass models.

In this study, we explain the binding energy of nucleons using the improved BW2 mass model by considering the higher-order term of the symmetry energy, which leads to the development of the BW3 mass model [37]. A set of model coefficients for the BW3 mass model was further tested and analyzed using multiple algorithms, aiming to improve the theoretical accuracy and extrapolation ability of the model. In order to verify the universality of the SLSQP algorithm, we applied it to 200 sample mass formulas. The results show that the SLSQP algorithm not only has stability and small root mean square error, but also high computational efficiency. Section 2 introduces the BW3 and $E_{isospin}$ mass models and sequential least squares programming. Section 3 is the performance of the SLSQP algorithm in enhancing the mass model. Section 4 provides a summary.

* The research at ZSTU was supported by the National Natural Science Foundation of China (Grants No.U2267205, No.12475124), a ZSTU intramural grant(22062267-Y), and Excellent Graduate Thesis Cultivation Fund (LW-YP2024011).

† Corresponding author,Hankui Wang, whk2007@163.com
‡ Corresponding author,Youbao Wang, ybwang@ciae.ac.cn

II. SEMI-EMPIRICAL MASS FORMULA

A. BW3 Mass model

The mass model of BW3 is derived from the droplet model and improves the semi-empirical mass formula [8–10] by incorporating additional physical constraints[37]:

$$\begin{aligned} B_{BW3} &= \alpha_V A + \alpha_S A^{2/3} + \alpha_C \frac{Z^2}{A^{1/3}} + \alpha_t \frac{(N-Z)^2}{A} \\ &+\alpha_{xC} \frac{Z^{4/3}}{A^{1/3}} + \alpha_W \frac{|N-Z|}{A} + \alpha_{st} \frac{(Z-N)^2}{A^{4/3}} \\ &+\alpha_p \delta(N,Z) A^{-1/2} + \alpha_R A^{1/3} + \alpha_m P + \beta_m P^2 \\ &+\alpha_{pm} \frac{(N-Z)^4}{A^3}. \end{aligned} \tag{1}$$

Eq.(1) involves 12 parameters, and the $\delta(N,Z)$ is defined as:

$$\delta(N,Z) = [(-1)^N + (-1)^Z]/2, \tag{2}$$

where 1 denotes even-even nuclei, -1 odd-odd nuclei, and 0 odd-A nuclei. P can be expressed as follows:

$$P = \frac{v_p v_n}{v_p + v_n}. \tag{3}$$

Here v_p (v_n) represents the difference between Z (N) and the magic number nearby.

$$\alpha_{pm} = \frac{1}{162} \left(\frac{9\pi}{8}\right)^{\frac{2}{3}} \frac{\hbar^2}{m r_0^2}. \tag{4}$$

Eq.(4) and its physical terms are derived from the application of the Fermi gas model to account for the nucleon binding energies. Following the restrictions of Pauli's exclusion principle, the nucleons (protons, neutrons, and nuclei) are assumed to move freely within the nuclear volume. The potential experienced by each nucleon is a superposition of the potentials created by other nucleons. Such a system of fermions is regarded as a degenerate gas, with temperatures below the Fermi temperature. The Fermi energy at 0 K is expressed as follows:

$$E_F = \frac{h^2}{2m} \left(\frac{3n}{8\pi}\right)^{\frac{2}{3}}, \tag{5}$$

where m represents the mass of the fermions, and n means their number density. The Fermi gas model gives the total kinetic energy of the nucleons as follows:

$$\begin{aligned} \langle E(Z,N)\rangle &= N\langle E_N\rangle + Z\langle E_Z\rangle \\ &= \frac{3}{10m}\frac{\hbar^2}{r_0^2} \left(\frac{9\pi}{4}\right)^{\frac{2}{3}} \left(\frac{N^{\frac{5}{3}} + Z^{\frac{5}{3}}}{A^{\frac{2}{3}}}\right). \end{aligned} \tag{6}$$

Assuming that the radii of the proton and neutron potential wells are identical, a binomial expansion near $N = Z$ yields the following expression:

$$\begin{aligned} \langle E(Z,N)\rangle &= \frac{3}{10m}\frac{\hbar^2}{r_0^2} \left(\frac{9\pi}{8}\right)^{\frac{2}{3}} [A + \frac{5}{9}\frac{(N-Z)^2}{A} \\ &+\frac{5}{243}\frac{(N-Z)^4}{A^3} + \cdots]. \end{aligned} \tag{7}$$

The first term contributes to the volume in the mass formula, whereas the second corrects for $N \neq Z$. The third term represents the higher-order addition to the symmetry energy used to enhance the mass model.

B. $E_{isospin}$ Mass model

The $E_{isospin}$ mass formula can be expressed by Strutinsky's theorem[35]:

$$E_{isospin}(Z,N) = -(E_{LDM} + \delta E). \tag{8}$$

Here, E_{LDM} is the macroscopic section and δE represents the fluctuating of the binding energy. The macroscopic section includes the volume term related to the isotopic spin, the Coulomb term, the surface term, the Coulomb energy correction term related to surface diffusion and the pairing term:

$$\begin{aligned} E_{LDM} &= \alpha_V \left[1 + \frac{4k_V T_z(T_z+1)}{A^2}\right] A \\ &+\alpha_S \left[1 + \frac{4k_S T_z(T_z+1)}{A^2}\right] A^{2/3} \\ &+\frac{3Z^2e^2}{5r_0 A^{1/3}} + \frac{\alpha_C Z^2}{A} + E_p. \end{aligned} \tag{9}$$

Here, a_V, k_V, a_S, k_S, a_C, and r_0 represent volume energy, isospin dependence of volume energy, surface energy, isospin dependence of surface energy, Coulomb energy, and Coulomb radius, respectively. T_Z is the third component of the isospin, and e is the electron charge. The smooth pairing energy is given by [38]

$$E_p = \begin{cases} \frac{\lambda_n}{N^{1/3}}, & Z \text{ even, } N \text{ odd,} \\ \frac{\lambda_p}{N^{1/3}}, & Z \text{ odd, } N \text{ even,} \\ \frac{\lambda_n}{N^{1/3}} + \frac{\lambda_p}{N^{1/3}} + \frac{\lambda_{np}}{N^{1/3}}, & Z, N \text{ odd,} \\ 0, & N, Z \text{ even.} \end{cases} \tag{10}$$

λ_n, λ_p, and λ_{np} are free parameters. The δE can be expressed as:

$$\begin{aligned} \delta E(\vec{x}) = \sum_{\vec{k}=\vec{0}}^{\vec{M}} \Big\{ & a_{\vec{k}} \cos\left(2\pi \frac{\vec{x}\cdot\vec{k}}{M}\right) \\ & + b_{\vec{k}} \sin\left(2\pi \frac{\vec{x}\cdot\vec{k}}{M}\right) \Big\}. \end{aligned} \tag{11}$$

Here $\vec{k} \equiv (k_1, k_2, k_3, k_4)$ ($0 \leq k_i \leq M$ for $i = 1, 2, 3, 4.$), and $\vec{x} \equiv (x_1, x_2, x_3, x_4)$:

$$\begin{aligned} x_1 = \beta_1 \left|\tfrac{N-N_o}{N}\right|, \quad x_2 = \beta_2 \left|\tfrac{Z-Z_o}{Z}\right|, \\ x_3 = \beta_3 N^{1/3}, \quad x_4 = \beta_4 Z^{1/3}. \end{aligned} \tag{12}$$

In this formula, $N_0(Z_0)$ is the magic number nearby. The β_1, β_2, β_3, and β_4 are the free parameters. The β_1 and β_2 describe the closeness to a shell closure given proton and neutron conditions, and β_3, and β_4 are proportional to Fermi momentum. The number of such parameters becomes quite large $(2M^4+4)$, while not all terms need to be expanded to M. so it can be simplified as:

$$\begin{aligned}\delta E(\vec{x}) &= \sum_{k_1=0}^{M}\sum_{k_2=0}^{M-k_1}\sum_{k_3=0}^{M-k_1-k_2}\sum_{k_4=0}^{M-k_1-k_2-k_3} \\ &\left\{a_{\vec{k}}\cos\left(2\pi\frac{\vec{x}\cdot\vec{k}}{M}\right)+b_{\vec{k}}\sin\left(2\pi\frac{\vec{x}\cdot\vec{k}}{M}\right)\right\}. \end{aligned} \quad (13)$$

It reduces the number of parameters to $\frac{1}{12}(M+4)!/M!+4$. Since the mean of δE is almost 0. Therefore, the free parameter can be further reduced to $\frac{1}{12}(M+4)!/M!+2$.

C. Algorithm Principles

This work study more than ten algorithms, namely Ordinary Least Squares (OLS) [39], SLSQP [36], Constrained Optimization by Linear Approximation (COBYLA) [40], Broyden-Fletcher-Goldfarb-Shanno (BFGS) [41], Conjugate Gradient (CG) [42], and so on. SLSQP, COBYLA, and Trust-Constr [43] were found to be better effective algorithms for solving constrained optimization problems (COPs). For solving the COP in Eq.(9), SLSQP was used because only SLSQP utilizes the information in the gradient and Hessian matrix [44] to the fullest extent, resulting in faster convergence to the optimal solution.

$$\begin{aligned} &\min && f(\vec{x}) \\ &st && g(\vec{x})=0, h(\vec{x})\geq 0 \\ &where && \vec{x}=(x_1,x_2,x_3,\ldots,x_{k-2},x_{k-1},x_k)\in X \\ & && X=\vec{x}|\vec{l}\leq\vec{x}\leq\vec{u} \\ & && \vec{l}=(l_1,l_2,l_3,\ldots,l_{i-2},l_{i-1},l_i) \\ & && \vec{u}=(u_1,u_2,u_3,\ldots,u_{j-2},u_{j-1},u_j). \end{aligned} \quad (14)$$

In this formula, $\vec{x}$ is the solution vector, X is the vector space of solution vectors, $\vec{l}$ ($\vec{u}$) is the upper (lower) bounds of the solution vector space, $g(\vec{x})$ is the equality constraint, $h(\vec{x})$ is the inequality constraint, and $f(\vec{x})$ is the objective optimization function [45].

The SLSQP algorithm iteratively minimizes the objective function under constraints through linear approximation. This transforms the nonlinear constrained problem into an unconstrained least squares problem. In each iteration, the gradient and Hessian matrix [44] are calculated to update the solution using Lagrange multipliers for the constraints.

$$L(\vec{x},\vec{\lambda},\vec{\mu})=f(\vec{x})+\vec{\lambda}^T*g(\vec{x})+\vec{\mu}^T*h(\vec{x}). \quad (15)$$

The superscript T denotes the transpose of the vector, $\vec{\lambda}$ and $\vec{\mu}$ represent the penalty terms associated with the equality and inequality conditions, respectively [46].

By solving the unconstrained least squares problem, an update rule is obtained for each iteration. This rule satisfies not only the equality and inequality constraints but also the first-order necessary conditions:

$$\nabla L(\vec{x},\vec{\lambda},\vec{\mu})=\nabla f(\vec{x})+J_g^T*\vec{\lambda}+J_h^T*\vec{\mu}=0, \quad (16)$$

J_g and J_h denote the Jacobian matrices of the equality and inequality constraints, respectively [47].

According to the above update rule, the initial value $\vec{x}_1$ is chosen and the stopping criterion ε is set. The gradient vector $\nabla f_k(\vec{x}_k)$ is computed at each iteration k. If $||\nabla f_k(\vec{x}_k)||<\varepsilon$, the algorithm is terminated, obtaining an approximate solution $\vec{x}^*$. This process constructs a sequential programming model as follows:

$$\begin{aligned} \min \quad & q(\vec{x})=f_k(\vec{x})+g_k^T(\vec{x}-\vec{x}_k) \\ & \quad +\frac{1}{2}(\vec{x}-\vec{x}_k)^T B_k(\vec{x}-\vec{x}_k) \\ st \quad & A_{eq}(\vec{x}-\vec{x}_0)=0 \\ & g_k(\vec{x})\geq 0, k=1,2,\ldots,k. \end{aligned} \quad (17)$$

In this formula B_k is a positive definite symmetric matrix used to approximate the inverse of the Hessian matrix, and A_{eq} is the Jacobian matrix of the equality constraints.

This model is solved to obtain the modified direction $\Delta\vec{x}$, computing the step size α such that the objective function sufficiently decreases along the search direction:

$$\begin{aligned} \alpha &= \min(1,r) \\ r &= \max(\beta_s,r_t) \\ \beta_s &= \left(\frac{\partial f}{\partial\vec{x}}\right)^T(\Delta\vec{x}/s) \\ r_t &= \left(\frac{\partial g}{\partial\vec{x}}\right)^T(\Delta\vec{x}/t), \end{aligned} \quad (18)$$

where s and t are positive scale factors. Finally, the estimated points are updated as follows: $\vec{x}_{k+1}=\vec{x}_k+\alpha\Delta\vec{x}$. By solving the above system of equations following this iterative process, the objective function is gradually optimized to determine the optimal solution that satisfies the constraints.

III. DISCUSSION

The coefficients of BW3 model is improved with less error between calculations and data by using SLSQP algorithm[36]. Subsequently, the following constraints are added to ensure the physical feasibility of the program calculations:

1. The nuclide numbers should satisfy $N\geq 8$ and $Z\geq 8$.
2. After satisfying Condition 1, the specific binding energy of the remaining nuclides, $\frac{B_{Th}}{N+Z}$, is distributed in the range of 5 - 9 MeV.

The performance metrics of the model were evaluated using RMSD [28], which is defined as follows:

$$RMSD=\sqrt{\frac{\sum_{i=1}^{n}(B_{Ex_i}-B_{Th_i})^2}{n}}, \quad (19)$$

TABLE 1. Coefficients of the BW3 mass model under each algorithm for binding energy (in MeV)

	OLS	SLSQP	BFGS	Trust-Constr	L-BFGS-B	CG
α_V	16.58	16.05	16.05	16.03	15.19	16.20
α_S	-26.95	-23.10	-23.10	-22.96	-16.47	-23.33
α_C	-0.774	- 0.74	- 0.74	- 0.74	- 0.71	-0.74
α_t	-31.51	-31.62	-31.62	-31.53	-25.83	-31.50
α_{xC}	2.22	1.59	1.59	1.59	1.42	1.39
α_W	-43.40	-72.96	-72.97	-72.14	5.39	-57.06
α_{st}	55.62	64.10	64.10	63.59	23.84	54.80
α_p	9.87	10.56	10.56	10.56	12.36	10.63
α_R	14.77	9.89	9.89	9.64	- 4.19	9.87
α_m	- 1.90	- 1.88	- 1.88	- 1.88	- 1.82	-1.89
β_m	0.14	0.14	0.14	0.14	0.14	0.14
α_{pm}	- 1.30	-11.36	-11.36	-11.31	- 1.13	0.14

where n represents the total number of nuclides involved in the calculation; B_{Ex_i} and B_{Th_i} are the current experimental and theoretical nuclide binding energies, respectively.

The modified coefficients are listed for some algorithms in Tab.I The different algorithms change the weights of the terms in the model, as shown in the table. The weights indicate the extent to which each term affects the model, and the symbols indicate positive or negative corrections. The volume, surface, symmetry, Wigner, surface symmetry, pairing, higher-order correction, and curvature terms have high weights because of their significant influence on the mass model, whereas the Coulomb, Coulomb exchange, and shell effect terms [21–27] have low weights because of their small influence. The horizontal coordinate of the plot is the number of neutrons N, and the vertical coordinate is the percentage of relative error [12] defined as

$$\frac{\delta B}{B}(\%) = \frac{B_{Ex} - B_{Th}}{B_{Ex}} * 100\%. \quad (20)$$

The errors exhibit different trends for different nuclide regions under different algorithms. Figs.1-a, 1-b, and 1-c show the reduction in the overall error and narrowing in the fluctuation range of the light and medium nuclide regions. In Figs.1-e and 1-f, the fluctuation amplitude of the heavy nuclide regions is improved, leading to an increase in the fluctuation amplitude of the light nuclide regions, such that the total RMSD does not improve or even deteriorate. SLSQP [36] exhibits greater advantages in reducing model errors when comparing performance metrics such as $\frac{\delta B}{B}(\%)$ [12] and RMSD [28] of the mass model obtained using different algorithms. This is attributed to the reduced weights of the surface and curvature terms by SLSQP and increased weights of Wigner, surface symmetry, pairing, and higher-order correction terms. The results also showed that in AME2020, the influence of the surface and curvature terms on the binding energy decreases, whereas the influence of the Wigner, surface symmetry, pairing, and higher-order correction terms on the overall effect increases. This also indicates that the impact of the surface and curvature terms on the binding energy is reduced, whereas the impact of the Wigner term on the overall effect increases. The mass model improves its extrapolation ability [17, 18] under

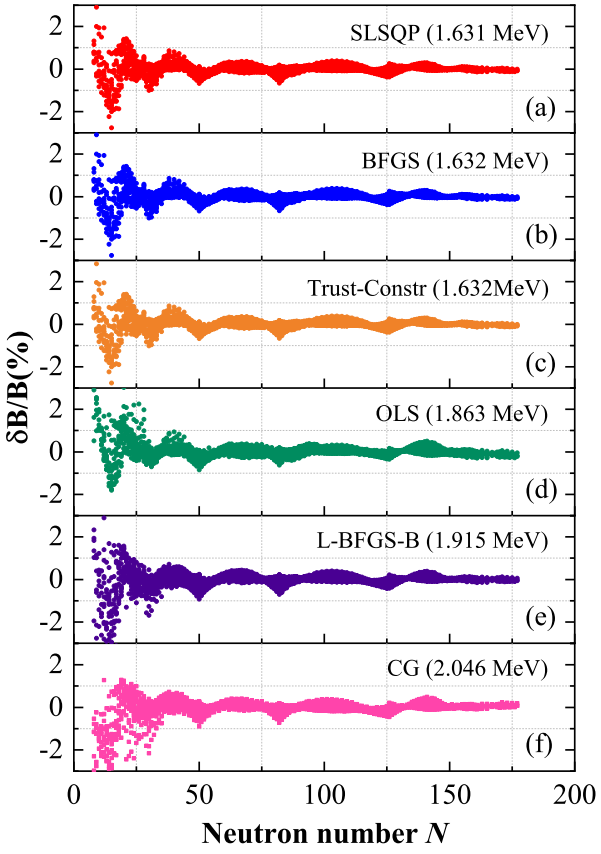

Fig. 1. BW3 mass model relative error comparison using different algorithms, and its RMSD is shown in parentheses.

SLSQP and more accurately reflects the contributions of the different physical terms to binding energy.

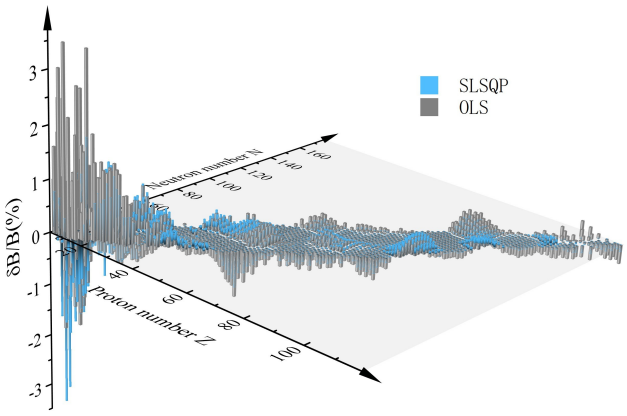

Fig. 2. BW3 mass model relative error comparison with SLSQP/OLS coefficients.

Fig.2 shows the relative error between the theoretical and experimental values of the BW3 mass model using the SLSQP and OLS algorithms, where the x-axis is the neutron number; the y-axis is the atomic number; and the z-axis is the relative error percentage $\frac{\delta B}{B}(\%)$. In the figure, the difference

fluctuations are more pronounced for the magic nuclei, especially in the nuclei surrounding the doubly magic nuclei, indicating different interactions between magic and non-magic nuclei. SLSQP improves the error near the doubly magic nuclei, captures the special interaction effects around the magic nuclei more accurately, and improves the accuracy of the theoretical model.

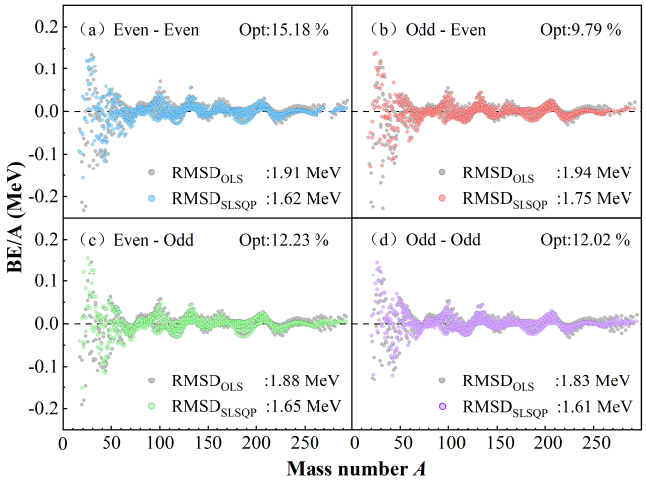

Fig. 3. BW3 mass model performance on total nuclei with SLSQP/OLS coefficients.

Fig.3 shows the performance of the SLSQP on even-even, odd-odd, and odd-A nuclei. The optimization effect of SLSQP on the different types of nuclei shows significant differences. The improvement is most significant in the case of even-even nuclei, and some optimization results can also be achieved in the case of odd-A and odd-odd nuclei. Fig.3-a shows that for even-even nuclei [48] (both Z and N are even), SLSQP provides a significant reduction in RMSD [28] by 0.29 MeV, with a performance improvement of about 15.18%, achieving a more substantial optimization in the whole nuclei region compared with the theoretical value of the BW3 model with OLS coefficients. In Fig.3-b, for odd-Z and even-N nuclei, after SLSQP optimization, the model RMSD is reduced by 0.19 MeV, with a performance improvement of approximately 9.79%. Similarly, in Fig.3-c, for even-Z and odd-N nuclei, the model RMSD is reduced by 0.23 MeV, with a performance improvement of approximately 12.23%. Notably, in the medium-nuclei region, the optimization results are closer to the experimental values. For odd-odd nuclei (both Z and N are odd), Fig.3-d shows that after SLSQP optimization, the model RMSD is reduced by 0.22 MeV and performance is improved by approximately 12.02%, particularly in the heavy nuclei region, where the optimization results are closer to the experimental values. These results further validate the effectiveness of SLSQP in mass model optimization.

The above method are only applicable to one nuclear mass formula. In order to verify its universality, we conducted a general discussion and applied the method to another multi-term nuclear mass formula. The results show that when optimizing the multi-term nuclear mass formula, SLSQP method performs better with smaller errors and faster convergence speed.

The $E_{isospin}$ mass model consists of two parts, the 5 terms based on the liquid drop model E_{LDM} with 9 free parameters, and the fluctuation term δE. Setting the degree of freedom M to 4, this formula will yield 153 parameters. Referring to the latest nuclear mass dataset AME2020, these parameters are optimized using Ordinary Least Squares (OLS), and the best value of the root mean square deviation is 1.268 MeV.

By studying the parameters, 62 parameters that have a significant impact on the model were selected. Using these 62 parameters as a sample set, 10 items were randomly selected to form a sample mass formula with the E_{LDM} item. This random process was repeated to obtain 200 sample mass formulas. Next, we used SLSQP, TRUST-CONST, BFGS and L-BFGS-B algorithms to optimize these mass formulas.

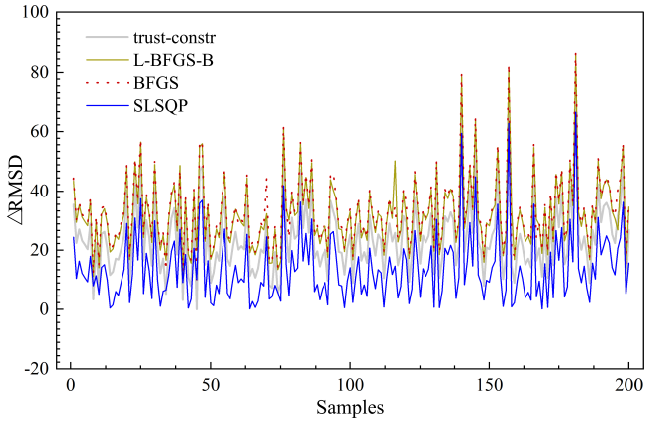

Fig. 4. Finding 62 important parameters from the δE term of $E_{isospin}$ mass model, randomly selecting 10 items as a sample formula with E_{LDM}, and obtaining 200 samples of mass formulas. The $\triangle RMSD$ is defined as $(RMSD - RMSD_{min}) * 100$, where $RMSD_{min}$ is the minimum root mean square deviation optimized by the algorithm for 200 samples.

As shown in Fig.4, the SLSQP algorithm is significantly better than the BFGS and L-BFGS algorithms. For example, for the 48th sample point, the $\triangle RMSD$ of SLSQP is 4 MeV, while that of BFGS and L-BFGS are 23.9 MeV and 23.0 MeV respectively. As the 67th sample point, the $\triangle RMSD$ of SLSQP is 2.7 MeV, while BFGS and L-BFGS are 22.7 MeV and 21.8 Mev respectively. For the TRUST-CONSTR algorithm, there is a large error amplitude which leads to poor stability in parameter optimization. In terms of computational efficiency compared to the SLSQP algorithm as a reference, it takes approximately 2.44 times longer in BFGS, 2.78 times longer in L-BFSG-B, and a staggering 8.44 times longer in trust algorithm. The SLSQP algorithm not only has good stability with small root mean square errors but also high computational efficiency.

To verify the effectiveness of the SLSQP, a comparison between experimental and theoretical values was conducted, as illustrated in Fig.5. The experimental binding energy (BE) values were obtained from the AME2020, while the theoretical values were predicted by optimizing the BW3 mass model using the SLSQP. Among the experimentally values,

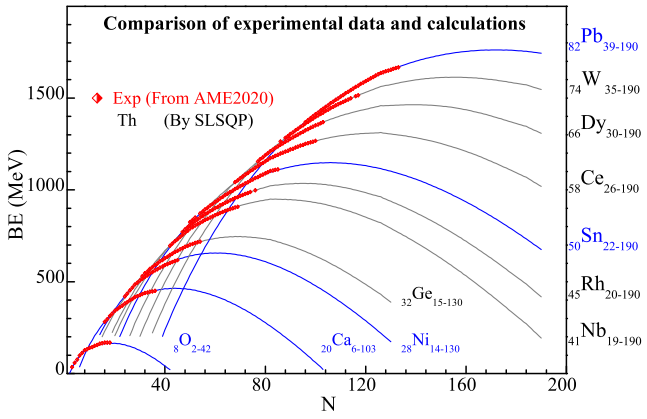

Fig. 5. Binding energy of Exp from the AME2020 [6, 7], and the theoretical predicted value by SLSQP method.

the maximum BE for O isotopes is currently measured at $^{24}O_{16}$ with BE = 168.95 MeV. Beyond this point, the BE decreases as the N increases. The SLSQP-optimized theoretical model predicts the maximum point at $^{26}O_{18}$ with BE = 168.95 MeV, followed by a similar decrease in BE with increasing N. For the other isotope chains, the experimentally BE values exhibit an overall increasing trend without reaching a maximum point. By optimizing the BW3 nuclear mass model with the SLSQP method, the following BE maximum points are predicted for these isotope chains: $^{64}Ca_{44}$ = 464.33 MeV, $^{88}Ni_{60}$ = 656.72 MeV, $^{123}Nb_{82}$ = 950.29 MeV, $^{141}Rh_{96}$ = 1035.66 MeV, $^{100}Ge_{68}$ = 745.77 MeV, $^{156}Sn_{106}$ = 1148.31 MeV, $^{184}Ce_{126}$ = 1311.84 MeV, $^{206}Dy_{140}$ = 1463.63 MeV, $^{230}W_{156}$ = 1613.36 MeV, $^{252}Pb_{170}$ = 1761.89 MeV.

IV. CONCLUSIONS

In this work, some algorithms are used to improve the accuracy of the mass model BW3. The SLSQP algorithm has the best performance in both root mean square errors and computational efficiency. This algorithm reduces the global RMSD from 1.863 MeV to 1.631 MeV (12.45% reduction). It enhances the precision of multinomial mass models. The odd (even) number of protons and neutrons are discussed, and SLSQP reduces the local RMSD from 1.91 MeV to 1.62 MeV (15.18% optimization), when nuclei have even numbers in both protons and neutrons. The local RMSD is reduced from 1.83 MeV to 1.61 MeV, when nuclei have odd numbers in both protons and neutrons. With odd (even) number of protons (neutrons), the local RMSD is reduced from 1.94 MeV to 1.75 MeV (9.79% optimization). The local RMSD is reduced from 1.88 MeV to 1.65 MeV (12.23% optimization), when proton number is even and neutron is odd. We further test these algorithms by 200 samples of mass formulas selecting from the δE term of $E_{isospin}$ mass model. The SLSQP shows a small error and fast convergence by comparison with other algorithms.

[1] B. Michael, P. H. Heenen, P. G. Reinhard, Self-consistent mean-field models for nuclear structure. Rev. Mod. Phys **75**, 121-180 (2003). https://doi.org/10.1103/RevModPhys.75.121

[2] D. Lunney, J. M. Pearson, and C. Thibault, Recent trends in the determination of nuclear masses. Rev. Mod. Phys **75**, 1021-1082 (2003). https://doi.org/10.1103/RevModPhys.75.1021

[3] A. C. Larsen, A. Spyrou, S. N. Liddick et al., Novel Techniques for Constraining Neutron-Capture Rates Relevant for r -Process Heavy-Element Nucleosynthesis. Prog. Part. Nucl. Phys **107**, 69-108 (2019). https://doi.org/10.1016/j.ppnp.2019.04.002

[4] T. Yamaguchi, H. Koura, M. Wang et al., Masses of exotic nuclei. Prog. Part. Nucl. Phys **120**, 103882 (2021). https://doi.org/10.1016/j.ppnp.2021.103882

[5] J. Erler, N. Birge, M. Kortelainen et al., The limits of the nuclear landscape. Nature **486**, 509-512 (2012). https://doi.org/10.1038/nature11188

[6] W. J. Huang, M. Wang, F. G. Kobdev et al., The AME 2020 atomic mass evaluation (I). Evaluation of input data, and adjustment procedures. Chinese. Phys. C **45**, 030002 (2021). https://doi.org/10.1088/1674-1137/abddb0

[7] M. Wang, W. J. Huang, F. G. Kobdev et al., The AME 2020 atomic mass evaluation (II). Tables, graphs and references. Chinese. Phys. C **45**, 030003 (2021). https://doi.org/10.1088/1674-1137/abddaf

[8] P. Möller, A. J. Sierk, T. Ichikawa et al., Nuclear ground-state masses and deformations: FRDM(2012). At. Data Nucl. Data Tables **109-110**, 1-204 (2016). https://doi.org/10.1016/j.adt.2015.10.002

[9] C. F. v. Weizsäcker, Leipzig, Zur Theorie der Kernmassen. Z. Physik **96**, 431-458 (1935). https://doi.org/10.1007/BF01337700

[10] H. A. Bethe, R. F. Bacher, Nuclear Physics A. Stationary States of Nuclei. Rev. Mod. Phys **8**, 82 (1936). https://doi.org/10.1103/RevModPhys.8.82

[11] B. Mohammed-Azizi, Better insight into the Strutinsky method. Phys. Rev. C **100**, 034319 (2019). https://doi.org/10.1103/PhysRevC.100.034319

[12] D. Benzaid, S. Bentridi, A. Kerraci et al., Bethe-Weizsacker semiempirical mass formula coefficients 2019 update based on AME2016. Nucl. Sci. Tech **31**, 9 (2020). https://doi.org/10.1007/s41365-019-0718-8

[13] W. H. Ye, Y. B. Qian, Z. Z. Ren, Accuracy versus predictive power in nuclear mass tabulations. Phys. Rev. C **106**, 024318 (2022). https://doi.org/10.1103/PhysRevC.106.024318

[14] P. Möller, W. D. Myers, H. Sagawa et al., New Finite-Range Droplet Mass Model and Equation-of-State Parameters. Phys. Rev. Lett **108**, 052501 (2012). https://doi.org/10.1103/PhysRevLett.108.052501

[15] H. Koura, T. Tachibana, M. Uno et al., Nuclidic Mass Formula on a Spherical Basis with an Improved Even-Odd Term. Prog. Theor. Phys **113**, 305 (2005). https://doi.org/10.1143/PTP.113.305

[16] F. A. Ivanyuk, K. Pomorski,Optimal shapes and fission barriers of nuclei within the liquid drop model. Phys. Rev. C **79**, 054327 (2009). https://doi.org/10.1103/PhysRevC.79.054327

[17] S. Goriely, N. Chamel, J. M. Pearson,Further explorations of Skyrme-Hartree-Fock-Bogoliubov mass formulas. XII. Stiffness and stability of neutron-star matter. Phys. Rev. C **82**, 035804 (2010). https://doi.org/10.1103/PhysRevC.82.035804

[18] S. Goriely, N. Chamel, Further explorations of Skyrme-Hartree-Fock-Bogoliubov mass formulas. XIII. The 2012 atomic mass evaluation and the symmetry coefficient. Phys. Rev. C **88**, 024308 (2013). https://doi.org/10.1103/PhysRevC.88.024308

[19] R. A. Rego, Mean free path in the relativistic mean field. Phys. Rev. C **44**, 1944 (1991). https://doi.org/10.1103/PhysRevC.44.1944

[20] J. L. Janssen, Y. Gillet, A. Martin et al., Precise effective masses from density functional perturbation theory. Phys. Rev. B **93**, 205147 (2016). https://doi.org/10.1103/PhysRevB.93.205147

[21] W. K. Michael, Mutual influence of terms in a semi-empirical mass formula. Nucl. Phys. A. **798**, 29-60 (2008). https://doi.org/10.1016/j.nuclphysa.2007.10.011

[22] D. M. William, J. S. Wladyslaw, Nuclear masses and deformations. Nucl. Phys **81**, 1-60 (1966). https://doi.org/10.1016/S0029-5582(66)80001-9

[23] A. N. Antonov, D. N. Kadrev, M. K. Gaidarov et al., Temperature dependence of the symmetry energy and neutron skins in Ni, Sn, and Pb isotopic chains. Phys. Rev. C **95**, 024314 (2017). https://doi.org/10.1103/PhysRevC.95.024314

[24] T. Naito, R. Akashi, H. Z. Liang, Application of a Coulomb energy density functional for atomic nuclei: Case studies of local density approximation and generalized gradient approximation. Phys. Rev. C **97**, 044319 (2018). https://doi.org/10.1103/PhysRevC.97.044319

[25] G. Lugones, A. G. Grunfeld, Surface and curvature properties of charged strangelets in compact objects. Phys. Rev. C **103**, 035813 (2021). https://doi.org/10.1103/PhysRevC.103.035813

[26] E. Wigner, On the Consequences of the Symmetry of the Nuclear Hamiltonian on the Spectroscopy of Nuclei. Phys. Rev **51**, 106 (1937). https://doi.org/10.1103/PhysRev.51.106

[27] R. F. Casten, Nuclear Structure from a Simple Perspective. Oxford. Acad **32**, 358-358 (2001). https://doi.org/10.1093/acprof:oso/9780198507246.001.0001

[28] G. Royer, C. Gautier, Coefficients and terms of the liquid drop model and mass formula. Phys. Rev. C **73**, 067302 (2006). https://doi.org/10.1103/PhysRevC.73.067302

[29] Z. M. Niu, H. Z. Liang, Nuclear mass predictions based on Bayesian neural network approach with pairing and shell effects. Phys. Lett. B **778**, 48-53 (2018). https://doi.org/10.1016/j.physletb.2018.01.002

[30] B. S. Cai, C. X. Yuan, Random forest-based prediction of decay modes and half-lives of superheavy nuclei. Nucl. Sci. Tech **34**, 204 (2023). https://doi.org/10.1007/s41365-023-01354-5

[31] Y. Y. Cao, J. Y. Guo, B. Zhou, Predictions of nuclear charge radii based on the convolutional neural network. Nucl. Sci. Tech **34**, 152 (2023). https://doi.org/10.1007/s41365-023-01308-x

[32] T. S. Shang, J. Li, Z. M. Niu, Prediction of nuclear charge density distribution with feedback neural network. Nucl. Sci. Tech **33**, 153 (2022). https://doi.org/10.1007/s41365-022-01140-9

[33] W. H. Ye, Y. B. Qian, H. K. Wang, Multiple constraints on nuclear mass formulas for reliable extrapolations. Phys. Rev. C **107**, 044302 (2023). https://doi.org/10.1103/PhysRevC.107.044302

[34] G. T. Garvey, W. J. Gerace, R. L. Jaffe et al., Set of Nuclear-Mass Relations and a Resultant Mass Table. Rev. Mod. Phys **41**, 1-80 (1969). https://doi.org/10.1103/RevModPhys.41.S1

[35] A. Bhagwat, Simple nuclear mass formula. Phys. Rev. C **90**, 064306 (2014). https://doi.org/10.1103/PhysRevC.90.064306

[36] M. Gong, F. Zhao, S. Y. Zeng et al., An experimental study on local and global optima of linear antenna array synthesis by using the sequential least squares programming. Appl. Soft. Comput. **148**, 110859 (2023). https://doi.org/10.1016/j.asoc.2023.110859

[37] X. Y. Xu, L. Deng, A. X. Chen et al., Improved nuclear mass formula with an additional term from the Fermi gas model. Nucl. Sci. Tech **35**, 91 (2024). https://doi.org/10.1007/s41365-024-01450-0

[38] P. Möller, J. R. Nix, Nuclear pairing models. Nucl. Phys. A **536**, 20-60 (1992). https://doi.org/10.1016/0375-9474(92)90244-E

[39] K. Lakshmi, B. Mahaboob, M. Rajaiah et al., Ordinary least squares estimation of parameters of linear model. J. Math. Comput. Sci. **11**, 2015-2030 (2021). https://doi.org/10.28919/jmcs/5454

[40] B. Rao, L. Yang, S. H. Zhong et al., Robust approximation of chance constrained optimization with polynomial perturbation. Comput. Optim. Appl. 1-27 (2024). https://doi.org/10.1007/s10589-024-00602-7

[41] F. Flachsenberg, M. Rarey, LSLOpt: An open-source implementation of the step-length controlled LSL-BFGS algorithm. J. Comput. Chem. **42**, 1095-1100 (2021). https://doi.org/10.1002/jcc.26522

[42] Y. L. Lu, W. Y. Li, C. M. Zhang et al., A Class New Hybrid Conjugate Gradient Method for Unconstrained Optimization. J. Comput. Chem. **12**, 1941-1949 (2015). https://api.semanticscholar.org/CorpusID:124611131

[43] Y. G. Pei, D. T. Zhu, On the Global Convergence of a Projective Trust Region Algorithm for Nonlinear Equality Constrained Optimization. Acta. Math. Sin.-English Ser. **34**, 1804-1828 (2018). https://doi.org/10.1007/s10114-018-7063-4

[44] P. G. Chen, Y. J. Peng, S. J. Wang, The Hessian matrix of Lagrange function. Linear. Algebra. Appl. **531**, 537-546 (2017). https://doi.org/10.1016/j.laa.2017.06.012

[45] F. S. P. S. Abad, M. Allahdadi, H. M. Nehi, Interval linear fractional programming: optimal value range of the objective function. Comp. Appl. Math **39**, 261 (2020). https://doi.org/10.1007/s40314-020-01308-2

[46] D. M. Hou, Y. X. Ning, C. Zhang, An efficient and robust Lagrange multiplier approach with a penalty term for phase-field models. J. Comput. Phys **488**, 112236 (2023). https://doi.org/10.1016/j.jcp.2023.112236

[47] P. Armand, N. N. Tran, Boundedness of the inverse of a regularized Jacobian matrix in constrained optimization and applications. Optim. Lett **16**, 2359-2371 (2022). https://doi.org/10.1007/s11590-021-01829-7

[48] Z. M. Niu, B. H. Sun, H. Z. Liang et al., Improved radial basis function approach with odd-even corrections. Phys. Rev. C **94**, 054315 (2016). https://doi.org/10.1103/PhysRevC.94.054315